Available online at www.sciencedirect.com

SciVerse ScienceDirect

Ceramics International 39 (2013) 6199–6206

CERAMICS INTERNATIONAL

www.elsevier.com/locate/ceramint

A CTAB-assisted hydrothermal synthesis of VO_2(B) nanostructures for lithium-ion battery application

Na Li[a], Wanxia Huang[a,*], Qiwu Shi[a], Yubo Zhang[a], Linwei Song[a]

[a]*College of Materials Science and Engineering, Sichuan University, Chengdu 610064, PR China*

Received 3 November 2012; received in revised form 8 January 2013; accepted 14 January 2013
Available online 23 January 2013

Abstract

Nanostructured VO_2(B) was synthesized via a combined hydrothermal method using V_2O_5 as a source material and oxalic acid powder as a reductant. Especially, cetyltrimethylammonium bromide (CTAB) was used as template and then three different morphologies of the VO_2(B): nanobelts, nanoflowers and nanoflakes were obtained through the change of the experimental conditions. The morphology and crystalline structure of the prepared products were characterized by scanning electron microscopy (SEM), X-ray diffraction (XRD), X-ray photoelectron spectroscopy (XPS) and Fourier transform infrared spectroscopy (FTIR). Furthermore, the electrochemical charge–discharge cycling properties of the VO_2(B) nanostructures in lithium-ion battery were investigated. The results indicated that the belt-like, flower-like and flake-like VO_2(B) nanostructures have the initial specific discharge capacity of 205.2, 254.0 and 56.0 mA h g^{-1}, and that the morphology of VO_2(B) nanostructures can deeply affect the service performance of batteries. According to the experiments, this CTAB-assisted hydrothermal method provides an insight into the preparation and application of nanostructured VO_2(B) as cathode material in lithium-ion battery.

Keywords: C. Electrical properties; D. Transition metal oxides; E. Batteries; E. CTAB

1. Introduction

Recently, low-dimensional (LD) nanostructured materials with different morphologies (nanotubes, nanorods, nanobelts, nanowires, etc.) have attracted a lot of attention because of their distinctive geometries as well as specific physical and chemical properties that are different from the bulk materials. On the basis of these novel properties, the nanostructured materials exhibit potential application in many areas such as electronics, optics, catalysis, mechanical and biomedical field [1,2].

Vanadium dioxide (VO_2) is an important binary compound mainly with five crystalline phases, including the most stable rutile-type VO_2(R), monoclinic VO_2(M), metastable VO_2(B), tetragonal VO_2(A) and VO_2(C) [3]. In the light of previous reports, the VO_2(R/M) has a fully reversible metal–semiconductor phase transition (MST) at 68 °C. Meanwhile, the optical transmittance and electrical resistivity have dramatic changes of 10^4–10^5 magnitude [4]. VO_2(A) is a metastable phase and its structure consists of a three-dimensional framework of VO_6 octahedra [5]. In addition, VO_2(B) is a metallic phase which is composed of distorted VO_6 octahedra sharing both corners and edges [6]. VO_2(B) has received special attention lately due to its typically layered structure and promising properties on the nanometer scale. For example, VO_2(B) is an attractive material that can serve as electrode material in lithium-ion batteries [2,6,7]. Because of these attractive properties and applications, various preparation methods of LD VO_2 nanostructures have been developed such as chemical vapor deposition [8,9], sol–gel [10,11], solution based method [12,13], thermolysis [14,15], pulsed laser ablation [16] and magnetron sputtering [17]. Among these, hydrothermal synthesis is found to be a suitable method to obtain VO_2(B). The benefits of this method were the lower required temperature, comparatively environmentally friendly reaction conditions, low cost, and simple operation.

*Corresponding author. Tel./fax: +86 28 85405781.
E-mail addresses: lnscu@yahoo.cn (N. Li), huangwanxiascu@yahoo.com.cn (W. Huang), shiqiwu_cd@yahoo.com.cn (Q. Shi), zhangyb920@gmail.com (Y. Zhang), linwei_s@yahoo.cn (L. Song).

0272-8842/$ - see front matter © 2013 Elsevier Ltd and Techna Group S.r.l. All rights reserved.
http://dx.doi.org/10.1016/j.ceramint.2013.01.039

More importantly, various morphologies of nanostructured materials can be obtained in the hydrothermal process. In addition, surfactants also have significant influence on the morphology of particles. For example, Ramimoghadam et al. synthesized ZnO nanostructures by the hydrothermal method using CTAB and sodium dodecyl sulfate (SDS) as structure directing agents [18]. Shi et al. used CTAB to form nanoporous structure in the VO_2 films [19].

In this paper, VO_2(B) nanostructures were fabricated by a facile and surfactant-assisted hydrothermal process. The raw materials for the synthesized process were vanadium pentoxide powder (V_2O_5), oxalic acid powder ($H_2C_2O_4\cdot 2H_2O$) and cationic surfactant cetyltrimethylammonium bromide (CTAB). According to the previous reports, different morphologies of VO_2(B) nanostructures can be fabricated by adjusting the concentration of oxalic acid solution [3,7]. However, in this experiment, suitable amount of CTAB was added into the reaction solution. The result demonstrated that CTAB played an important role as a soft template in affecting the morphologies of the nanostructured VO_2(B). Finally, VO_2(B) nanostructures with three types of morphologies were synthesized smoothly. Besides, the electrochemical experiments were conducted in order to present charge–discharge capacity of the as-prepared VO_2(B) nanostructures in lithium-ion battery.

2. Experimental section

2.1. Synthesis of VO_2(B)

The raw materials for hydrothermal procedure were vanadium pentoxide (V_2O_5), $H_2C_2O_4\cdot 2H_2O$ solid powder and cetyltrimethylammonium bromide (CTAB). All chemicals were of analytical grade and used without further purification. A mixture of 1.092 g V_2O_5 powder, suitable amount of $H_2C_2O_4\cdot 2H_2O$ powder (0.756, 1.512 or 2.268 g) and CTAB (0.08, 0.06 or 0.04 g) was added to 70 ml de-ionized water directly at room temperature. The mixed solution was stirred continuously for 2 h. Then a yellow-green suspension liquid was formed. The liquid was transferred into a 100 ml autoclave with a Teflon liner quickly and then maintained at 180 °C for 36 h or 48 h without shaking and stirring. After cooling naturally from high temperature to room temperature, dark blue precipitate was obtained from the solution by centrifugation. It was washed with de-ionized water and absolute ethanol for several times and dried at 80 °C for 18 h in a thermostatic drying oven. Table 1 shows the summary of three experimental conditions. The probable reaction in the hydrothermal treatment could be revealed as following:

$$V_2O_5 + H_2C_2O_4\cdot 2H_2O \rightarrow 2VO_2 + 2CO_2 + 3H_2O \quad (1)$$

Table 1
The experimental conditions of VO_2(B) nanostructures.

	V_2O_5:$H_2C_2O_4\cdot 2H_2O$ (molar ratio)	CTAB (g)	Temperature (°C)	Reaction time (h)
1	1:1	0.08	180	48
2	1:2	0.06	180	36
3	1:3	0.04	180	48

2.2. Characterization

The morphologies of products were investigated by S-4800 field emission scanning electron microscopy (FESEM, Hitachi). The crystalline structures of as-prepared VO_2(B) were measured by DX2000 X-ray powder diffraction (XRD) with Cu Kα radiation ($\lambda=0.154056$ nm). The vanadium valence states of the materials were determined by X-ray photoelectron spectroscopy (XPS) (Kratos, England) with Al Kα ($hv=1486.6$ eV) exciting source. Fourier-transform infrared spectrum (FTIR) was recorded in the range of 400–4000 cm^{-1} using a Tensor 27 (Bruker, Germany) spectrometer. Specific surface area (BET), total pore volume and average pore radius of different powders were measured with a Quadrasorb SI (Quantachrome) instrument, using adsorption and desorption of N_2 at the temperature of liquid nitrogen.

2.3. Electrochemical measurement

For investigating the electrochemical properties of the obtained VO_2(B) nanostructures, a mixture of VO_2(B) samples (80 wt%), acetylene black (10 wt%) and polyvinylidene fluoride (PVDF, 10 wt%) was dissolved in N-methylpyrrolidone (NMP) solution and coated on aluminum foil. Then it was cut into disc electrodes with a diameter of 14 mm by punch. In the test, typical coin-type cells (2025) were used and assembled in an argon-filled glove box where water and oxygen concentration were kept lower than 1 ppm. Celgard 2325 was used as a separator membrane. The electrolyte solution was composed of ethylene carbonate (EC), dimethyl carbonate (DMC) and ethylene methyl carbonate (EMC) in 1:1:1 (volumetric ratio), in which 1 mol L^{-1} $LiPF_6$ was dissolved. The charge–discharge curves were tested using the Land battery system (CT2001A) at a current density of 20 or 200 mA g^{-1} with a voltage region between 1.5 V and 4 V. Electrochemical impedance spectroscopy (EIS) measurement was carried out in the 100 kHz to 10 mHz frequency range using the Parstat 2273 (Princeton Inc.) electrochemical workstation at 25 °C.

3. Results and discussion

3.1. Morphology and structure

The morphologies of as-synthesized VO_2(B) nanostructures are shown in Fig. 1(a) and (b). Fig. 1(a) shows the SEM image of VO_2(B) nanobelts, it is fabricated with 1:1 (molar ratio) of V_2O_5 and oxalic acid at 180 °C for 48 h, without CTAB addition. In accordance with the result of the image, the VO_2(B) nanobelts obviously have agglomeration and

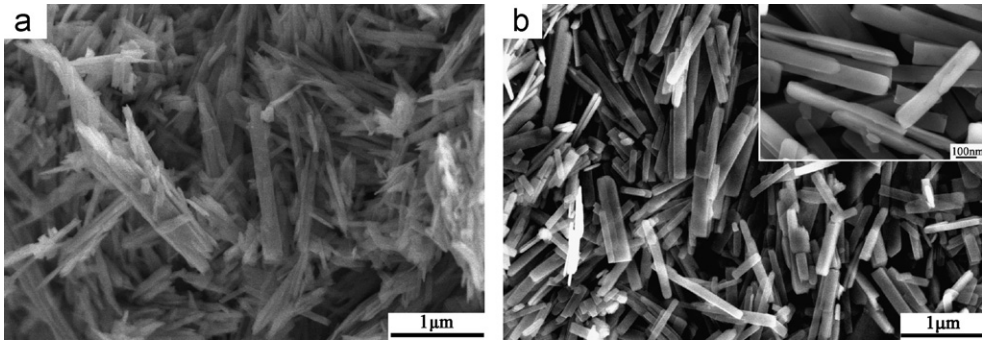

Fig. 1. SEM images of VO_2(B): (a) nanobelts (V_2O_5:$H_2C_2O_4 \cdot 2H_2O$ molar ratio 1:1, without CTAB addition) and (b) nanobelts (V_2O_5:$H_2C_2O_4 \cdot 2H_2O$ molar ratio 1:1, with 0.08 g CTAB addition).

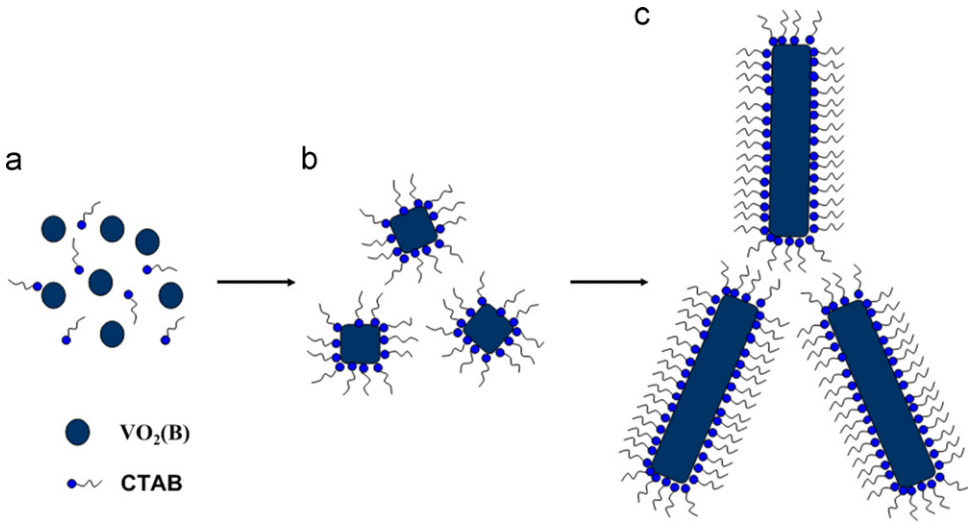

Fig. 2. Schematic diagram for the VO_2(B) nanobelts formation mechanism with CTAB addition.

some fragments. Fig. 1(b) presents the SEM image of VO_2(B) nanobelts synthesized with 1:1 (molar ratio) of V_2O_5 and oxalic acid and 0.08 g CTAB at 180 °C for 48 h. The SEM observation shows that the as-prepared VO_2(B) nanobelts have regular crystal structure, excellent dispersibility and no obvious agglomeration. Inset of Fig. 1(b) presents that nanobelts are of rectangular cross-section with length 1–2 μm, width 80–100 nm and thickness 30–60 nm. And the morphology characterization is much better than that of nanostructured VO_2(B) which is shown in Fig. 1(a). In the experiments, CTAB is used as structure-directing template that generally plays a key role in the synthesis of nanostructured materials. The existence of surfactant can reduce the surface tension and energy when a new phase in the solution is formed. In the meantime, the solution can obtain a lower supersaturation which is beneficial to anisotropic or one-dimensional growth of the crystals [2]. CTAB is an amphiphilic coupling agent and has a functional structure in which one end is hydrophilic but the other one is hydrophobic. Therefore CTAB presents self-agglomeration behavior in the hydrothermal system [19]. On the basis of previous experimental observation, a schematic diagram of the mechanism is showed in Fig. 2(a)–(c). In the formation process of VO_2(B) crystal nucleus, the hydrophilic ends of CTAB will bond with water while the hydrophobic ends around the VO_2(B) crystal nucleus (Fig. 2(a)). With the reaction proceeding continuously, the VO_2(B) particles will assemble together and grow (Fig. 2(b)). Finally, the VO_2(B) nanobelts are formed (Fig. 2(c)). In the reaction solution, CTAB has an influence on the growth direction of VO_2(B) nanoparticles through the self-agglomeration behavior. Moreover, surfactant CTAB may play a certain function as a growth controller, as well as an agglomeration inhibitor, by forming a covering film on the VO_2(B) nanobelt [20].

After changing the molar ratio of V_2O_5 and oxalic acid (1:2) and the amount of CTAB and reaction time, another kind of VO_2(B) nanostructure was obtained. As shown in Fig. 3(a), the product consists of a large number of flower-like nanostructures. The diameter of these nanoflowers is about 10–15 μm. Moreover, the inset indicates that the nanoflowers are self-assembled by a large quantity of VO_2(B) nanobelts with the length of 1–2 μm. It is quite interesting that these nanobelts were connected together at the center and grew along the radial direction. According to the experimental phenomenon, the possible reason was that the changed reaction system moved to a state with

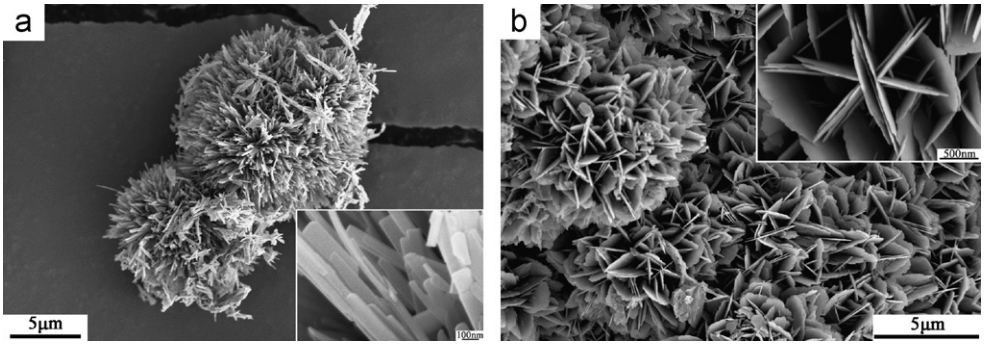

Fig. 3. SEM images of VO_2(B): (a) nanoflowers and (b) nanoflakes.

lower total energy, which contributed to the nanobelts tend to assemble to form flower-like VO_2(B).

When the molar ratio (V_2O_5:$H_2C_2O_4 \cdot 2H_2O$) increased to 1:3, flake-like and snowflake-like nanostructures were obtained as shown in Fig. 3(b). Inset is a single snowflake-like VO_2(B) nanostructure that is about 2 μm in diameter. The SEM image reveals that the snowflake-like VO_2(B) is composed of several nanoflakes with the thickness of about 10–15 nm. So far, there are still no detailed mechanisms for the formation of the nanostructures in the hydrothermal process. But no matter how complicated the reasons are, the concentration of $H_2C_2O_4 \cdot 2H_2O$ and CTAB could have great effects on the synthesis of morphology-controlled VO_2(B) nanostructures.

Fig. 4(a)–(c) presents the XRD patterns of VO_2(B) nanobelts, nanoflowers and nanoflakes. Most of the peaks are rapidly indexed to VO_2(B) phase (space group: C2/m, JCPDS no. 81-2392) with lattice constants of $a=12.093$ Å, $b=3.702$ Å, $c=6.433$ Å and $\beta=107.0^\circ$. However, there are some extra peaks existing in the XRD patterns corresponding to impurities of V_2O_3 and V_2O_5. This is because hydrothermal synthesis is a complicated and mild reaction process and there are many experimental factors that can have much influence on results of the experiment mainly including the molar ratio of materials and hydrothermal treatment temperature. The strong and sharp diffraction peaks of the XRD image exhibit the well-crystallized prepared particles. In addition, slight differences can be found according to the relative intensity of diffraction peaks. Comparing the three patterns, Fig. 4(b) has sharper peak suggesting a relatively higher crystallinity and preferential orientation along (110).

In order to understand the detailed compositions and valence states of the products, a typical XPS measurement was carried out for the as-prepared powders. Fig. 5(a) displays a typical wide range survey spectrum of the VO_2(B) nanostructures, revealing the presence of vanadium, oxygen, carbon and nitrogen. The peak of C could be attributed to the CO_2 adsorbed on the surface of the sample or the contaminant from the conductive carbon tape used to bind the powders. Then the vanadium valence states of the samples with three different morphologies were detected by fitting the peak position of $V2p_{3/2}$ using a Shirley function with the XPS Peak

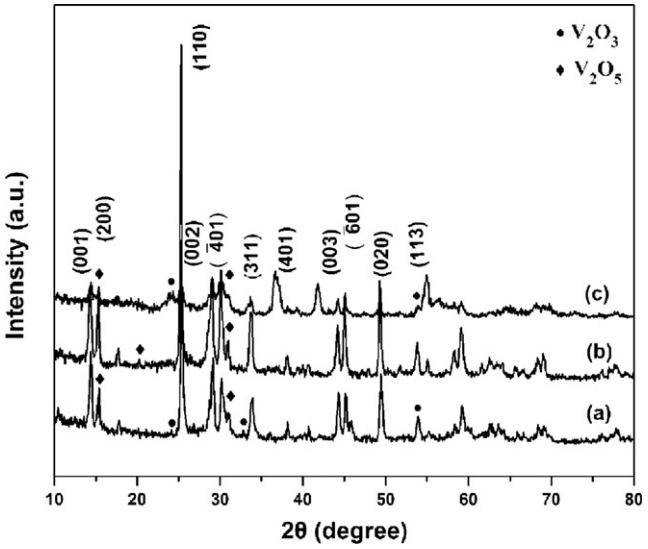

Fig. 4. XRD patterns of the VO_2(B): (a) nanobelts; (b) nanoflowers; and (c) nanoflakes.

4.1 software, as shown in Fig. 5(b–d). In Fig. 5(b) and (d), the XPS spectra of the nanobelts and nanoflakes present three valence states of vanadium, +5 valence (with a binding energy of 516.9–517.7 eV), +4 valence (with a binding energy of 515.7–516.2 eV) and +3 valence (with a binding energy of 515.2–515.9 eV) [21]. In Fig. 5(c), the XPS spectrum of the nanoflowers exhibits two valence states of vanadium, +5 valence and +4 valence. According to the analyzed XPS spectra, the fractional percentages of the V^{5+}, V^{4+}, V^{3+} valence states for the as-obtained products can be evaluated as 42.9%, 45.4% and 11.7% (b), 53.5% and 46.5% (c), 34.4%, 43.0% and 22.6% (d). Other vanadium oxides can be seen in the as-prepared samples, which is consistent with the result of XRD. Fig. 5(c) shows the sample that includes two vanadium valence states but without V^{3+} due to the effect of different reaction times. The nanobelts and nanoflakes were synthesized at 180 °C for 48 h. The nanoflowers were obtained at 180 °C for only 36 h in hydrothermal system. Besides the reaction time, the reducing agent also has obvious influence during the formation of the final products. The nanobelts and nanoflakes were obtained when the molar ratios of V_2O_5 and oxalic acid were 1:1 and 1:3. Therefore comparing the results, the

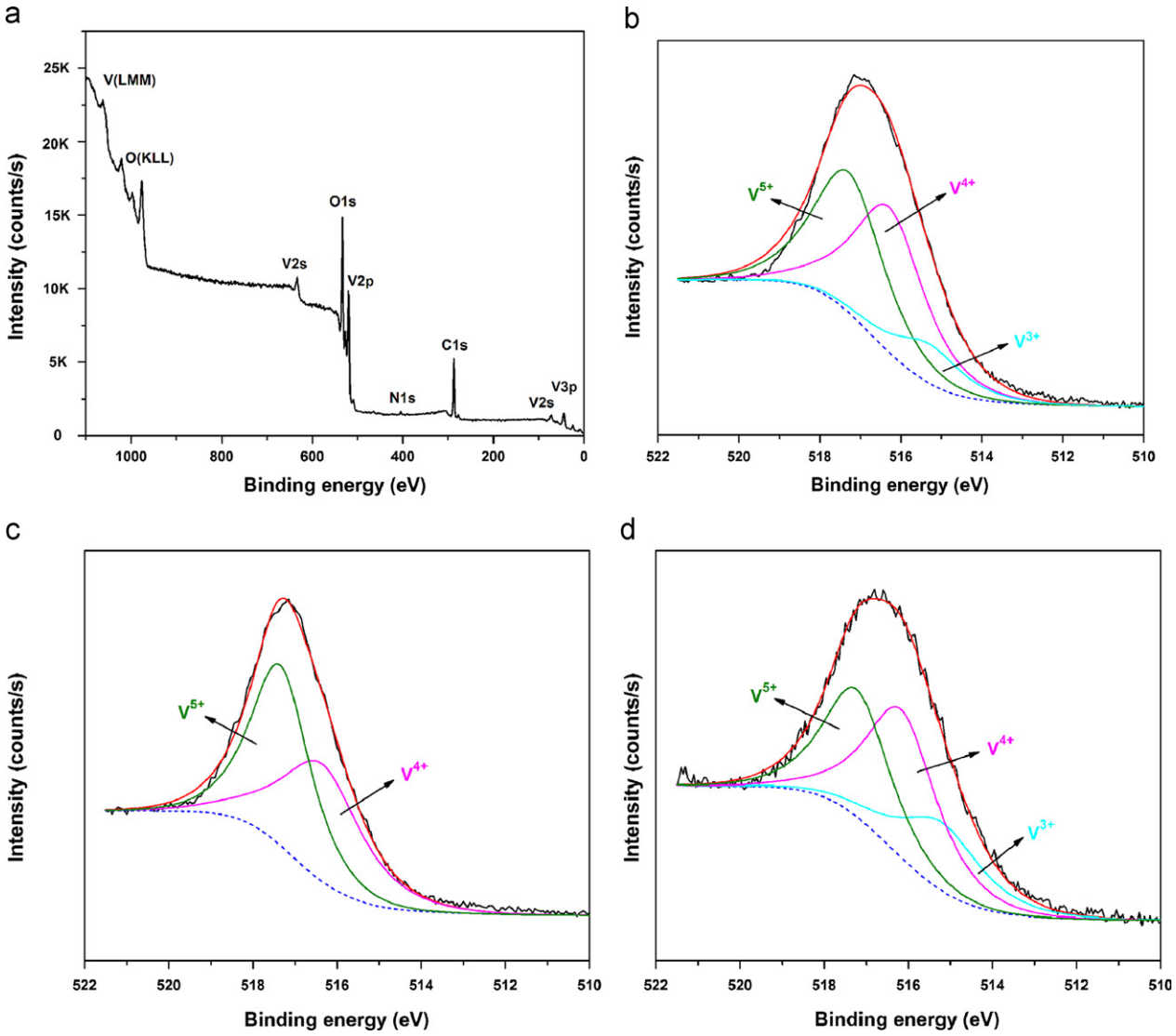

Fig. 5. XPS of VO_2(B) nanostructures: (a) wide range survey spectrum; high-resolution scans of V2p for the nanobelts (b), nanoflowers (c) and nanoflakes (d).

fractional percentage of V^{3+} in Fig. 5(d) was higher than that in Fig. 5(b).

Fig. 6 shows the typical IR spectrum of VO_2(B) nanostructures. According to previous reports, IR peaks between 400 and 1000 cm^{-1} can be ascribed to all kinds of vibrations of V–O type [13]. The 1001 cm^{-1} band detected from VO_2(B) can be observed in many vanadium oxide compounds with intermediate oxidation state between V^{5+} and V^{4+} ions, which is attributed to the stretching of the short V═O bonds [22]. There is a weak band at 924 cm^{-1} that is assigned to the coupled vibration between V═O and V–O–V. The broad vibrational bands at 548 cm^{-1} can be correlated with V–O–V octahedral bending modes.

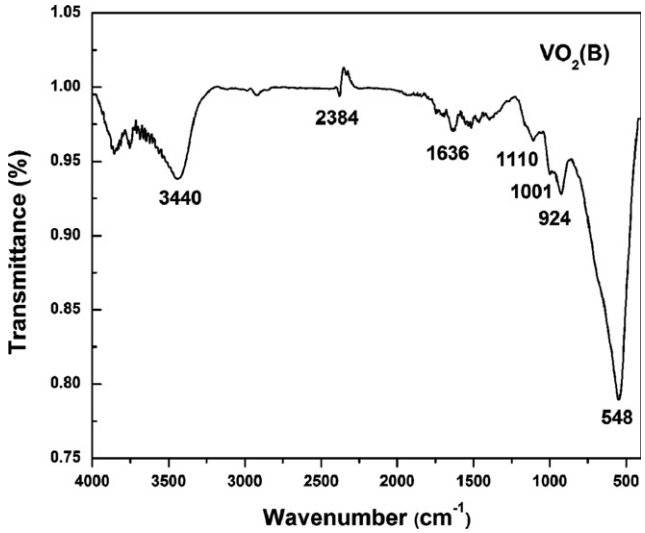

Fig. 6. FT-IR spectrum of the as-synthesized VO_2(B).

3.2. Electrochemical performance

The tunnel size (4.984 Å × 3.281 Å) of VO_2(B) is obviously larger than the diameter of lithium ion (3.281 Å). In light of

the fascinating property, it can improve the Li-ion diffusion through the crystal structure. Consequently the electrochemical reaction can be facilitated [7]. Here we discuss the three morphologies of VO_2(B) nanostructures as the candidate cathode material applied in lithium-ion battery. The electrochemical properties of the three morphologies of VO_2(B) are presented in Fig. 7. The specific discharge capacities about the first cycle for the belt-like, flower-like and flake-like VO_2(B) are 205.2, 254.0 and 56.0 mA h g^{-1} respectively, as shown in Fig. 7. According to comparison of the initial discharge curves, it can be clearly found that the nanobelts electrode has not only a better specific discharge capacity but also a flatter and longer voltage plateau at near 2.5 V than electrodes with other morphologies, which is necessary for lithium-ion battery application to achieve a larger extent of Li-ion intercalation and deintercalation [23]. In the case of VO_2(B) nanoflowers

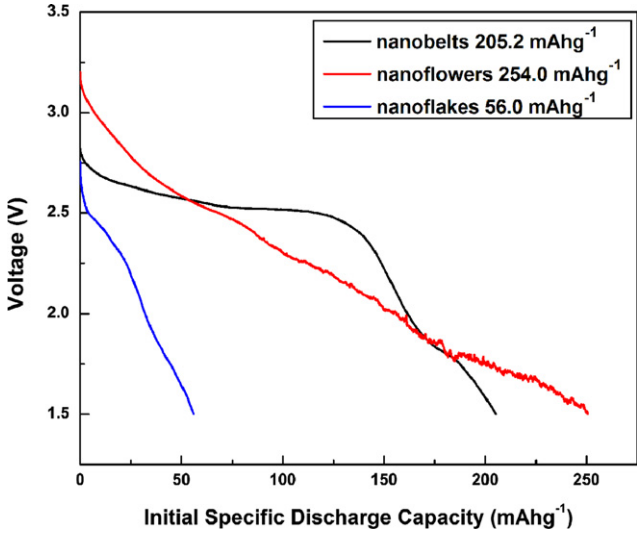

Fig. 7. Voltage versus specific discharge capacity curves for VO_2(B) nanobelts, nanoflowers and nanoflakes during the first cycle with a current density of 20 mA g^{-1}.

electrode, it has a higher specific discharge capacity than that of belt-like VO_2(B) but without a distinct voltage plateau which is an important standard to evaluate the quality of lithium-ion battery. However, according to the test data, the initial specific discharge capacities of VO_2(B) nanobelts and nanoflowers are much better than the previous reports of VO_2(B) nanostructures [2,24,25]. Fig. 8(a) illustrates the cycle performance of VO_2(B) nanobelts. The specific capacity is 138.9 mA h g^{-1} after 30 cycles which is 67.7% of the first specific discharge capacity at a current density of 20 mA g^{-1}. Moreover, it can still deliver 186.3 mA h g^{-1} lithium ion at a relatively high current density of 200 mA g^{-1} and the capacity retention is 65.5% after 30 cycles. The capacity decreased with increasing current density is derived from the resistance of the VO_2(B) electrode. Fig. 8(b) exhibits the electrochemical impedance spectrum (EIS) of VO_2(B) nanobelts. In accordance with the point intersecting with the real axis at high frequencies range, the internal resistance of nanobelts electrode is about 23 Ω. As can be seen, the impedance plot shows one semicircle in medium-frequency region which could be due to the charge-transfer resistance and a line in low-frequency range which could be attributed to Warburg impedance [26]. Based on the known experimental test results, there are V^{3+} and V^{5+} existing in the as-obtained samples. Through comparing the fractional percentages of V^{5+}, V^{4+}, and V^{3+} valence states of the products, it is found that the relative contents of compositions do not have obvious differences. Moreover, the nanobelts and nanoflakes display similar compositions but significantly different initial discharge capacities. This means that various morphologies of the similar substance may also lead to different properties. Table 2 shows that the specific BET surface areas of nanobelts, nanoflowers and nanoflakes are 10.83, 18.71 and 5.196 m^2 g^{-1}. Liu et al. prepared hollow spherical VO_2(B) material by the hydrothermal method, its specific BET surface area reaches 13.02 m^2 g^{-1} and its initial discharge capacity is 450 mA h g^{-1} when recored at the current density of 10 mA g^{-1} [27]. It is known to all that

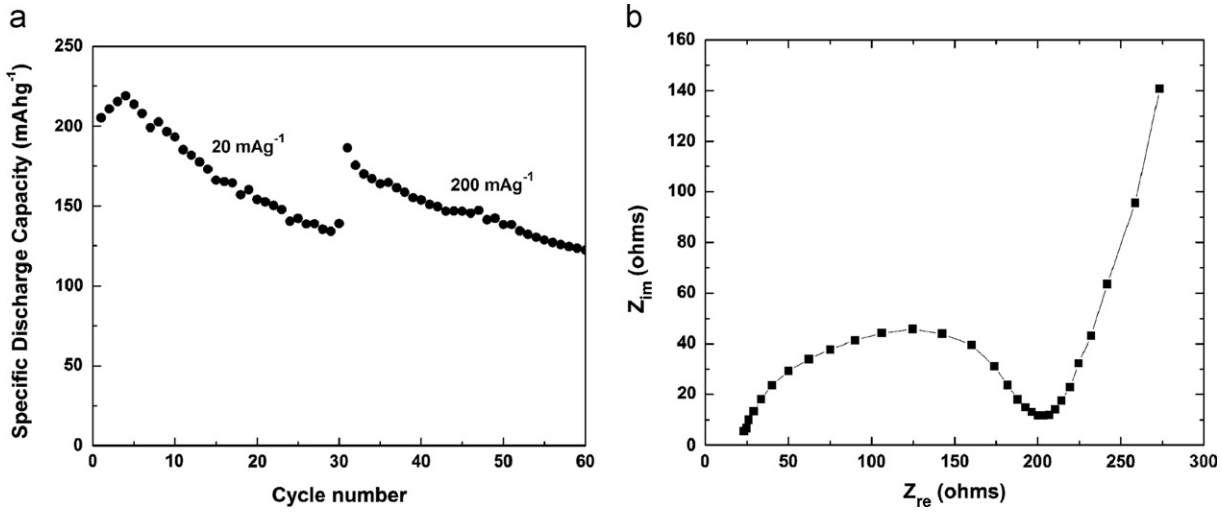

Fig. 8. (a) Corresponding cycling performance of VO_2(B) nanobelts at a current density of 20 or 200 mA g^{-1} and (b) electrochemical impedance spectrum of the nanaobelts VO_2(B) electrode.

Table 2
The BET surface area, total pore volume and average pore radius analysis of VO_2(B) nanostructures.

	BET surface area ($m^2\ g^{-1}$)	Total pore volume ($cm^3\ g^{-1}$)	Average pore radius (Å)
Nanobelts	10.83	0.02988	55.18
Nanoflowers	18.71	0.05718	61.11
Nanoflakes	5.196	0.01222	47.05

many chemical and physical properties of products deeply depend on both initial material size and synthetic method. The good initial discharge capacity of VO_2(B) nanobelts may be relevant to the uniquely synthetic environment in hydrothermal approach and high surface-to-volume ratio due to special morphology [6]. Huynh et al. reported that the operating properties of a battery depend not only on the structure but also on the morphology of the electrode components [28]. However, large specific surface areas and high surface energy also lead VO_2(B) nanoscale materials to aggregate together easily during charge–discharge test, thus increasing the charge transfer resistance and causing a poor cycling performance [29]. In addition, the crystallinity of electrode materials also limits the practical application of lithium-ion battery [23].

4. Conclusion

In summary, three different morphologies of VO_2(B): nanobelts, nanoflowers and nanoflakes had been fabricated via a facile and surfactant-assisted hydrothermal synthesis, using V_2O_5 as a source of vanadium, oxalic acid as a reductant and cetyltrimethylammonium bromide (CTAB) as a template. Based on the experimental results and data analysis, the morphologies can be influenced by changes in experimental conditions: the amount of oxalic acid and CTAB and reaction time. Moreover, electrochemical properties of as-obtained VO_2(B) nanobelts, nanoflowers and nanoflakes as electrode materials of lithium-ion battery are investigated by charge–discharge test. The belt-like VO_2(B) nanostructure has better specific discharge capacity of 205.2 mA h g^{-1} when comparing with other samples, indicating that it has the potential to be applied in lithium-ion battery as cathode electrode materials.

Acknowledgments

This work was financially supported by the National Natural Science Foundation of China (Grant no. 61271075), and the Cooperative Innovation Mutual Foundation of China Academy of Engineering Physics and Sichuan University (Grant no. 0082604132225).

References

[1] S.D. Ji, Y.G. Zhao, F. Zhang, P. Jin, Direct formation of single crystal VO_2(R) nanorods by one-step hydrothermal treatment, Journal of Crystal Growth 312 (2010) 282–286.
[2] N. Ganganagappa, A. Siddaramanna, One step synthesis of monoclinic VO_2(B) bundles of nanorods: cathode for Li ion battery, Materials Characterization 68 (2012) 58–62.
[3] H.H. Yin, K. Yu, Z.L. Zhang, Z.Q. Zhu, Morphology-control of VO_2(B) nanostructures in hydrothermal synthesis and their field emission properties, Applied Surface Science 257 (2011) 8840–8845.
[4] K.F. Zhang, X. Liu, Z.X. Su, H.L. Li, VO_2(R) nanobelts resulting from the irreversible transformation of VO2(B) nanobelts, Materials Letters 61 (2007) 2644–2647.
[5] Y. Oka, T. Yao, N. Yamamoto, Powder X-ray crystal structure of VO_2(A), Journal of Solid State Chemistry 86 (1990) 116–124.
[6] S.B. Ni, H.B. Zeng, X.L. Yang, Fabrication of VO_2(B) nanobelts and their application in lithium ion batteries, Journal of Nanomaterials 2011 (2011) 961389.
[7] J. Ni, W.T. Jiang, K. Yu, Y.F. Gao, Z.Q. Zhu, Hydrothermal synthesis of VO_2(B) nanostructures and application in aqueous Li-ion battery, Electrochimica Acta 56 (2011) 2122–2126.
[8] T. Maruyama, Y. Ikuta, Vanadium dioxide thin films prepared by chemical vapour deposition from vanadium (III) acetylacetonate, Journal of Materials Science 28 (1993) 5073–5078.
[9] T.D. Manning, I.P. Parkin, M.E. Pemble, D. Sheel, D. Vernardou, Intelligent window coatings: atmospheric pressure chemical vapor deposition of tungsten-doped vanadium dioxide, Chemistry of Materials 16 (2004) 744–749.
[10] D.C. Yin, N.K. Xu, J.Y. Zhang, X.L. Zheng, Vanadium dioxide films with good electrical switching property, Journal of Physics D: Applied Physics 29 (1996) 1051–1057.
[11] N.Y. Yuan, J.H. Li, C.L. Lin, Valence reduction process from sol–gel V_2O_5 to VO_2 thin films, Applied Surface Science 191 (2002) 176–180.
[12] S.A. Corr, M. Grossman, Y.F. Shi, K.R. Heier, G.D. Stucky, R. Seshadri, VO_2(B) nanorods: solvothermal preparation, electrical properties, and conversion to rutile VO_2 and V_2O_3, Journal of Materials Chemistry 19 (2009) 4362–4367.
[13] F. Sediri, N. Gharbi, Controlled hydrothermal synthesis of VO_2(B) nanobelts, Materials Letters 63 (2009) 15–18.
[14] Z.F. Peng, W. Jiang, H. Liu, Synthesis and electrical properties of tungsten-doped vanadium dioxide nanopowders by thermolysis, Journal of Physical Chemistry C 111 (2007) 1119–1122.
[15] C.M. Zheng, J.L. Zhang, G.B. Luo, J.Q. Ye, M.M. Wu, Preparation of vanadium dioxide powders by thermolysis of a precursor at low temperature, Journal of Materials Science 35 (2000) 3425–3429.
[16] D.H. Kim, H.S. Kwok, Pulsed laser deposition of VO_2 thin films, Applied Physics Letters 65 (1994) 3188–3190.
[17] X.J. Wang, H.D. Li, Y.J. Fei, X. Wang, Y.Y. Xiong, Y.X. Nie, K.A. Feng, XRD and Raman study of vanadium oxide thin films deposited on fused silica substrates by RF magnetron sputtering, Applied Surface Science 177 (2001) 8–14.
[18] D. Ramimoghadam, M.Z.B. Hussein, Y.H. Taufig-Yap, The effect of sodium dodecyl sulfate (SDS) and cetyltrimethylammonium bromide (CTAB) on the properties of ZnO synthesized by hydrothermal method, International Journal of Molecular Sciences 13 (2012) 13275–13293.
[19] Q.W. Shi, W.X. Huang, Y.J. Xu, Y.X. Zhang, F. Yue, S. Qiao, S.P. Zheng, J.Z. Yan, Synthesis and terahertz transmission properties of nano-porous vanadium dioxide films, Journal of Physics D: Applied Physics 45 (2012) 385302.
[20] X.M. Sun, X. Chen, Z.X. Deng, Y.D. Li, A CTAB-assisted hydrothermal orientation growth of ZnO nanorods, Materials Chemistry and Physics 78 (2002) 99–104.
[21] X.H. Liu, G.Y. Xie, C. Huang, Q. Xu, Y.F. Zhang, Y.B. Luo, A facile method for preparing VO_2 nanobelts, Materials Letters 62 (2008) 1878–1880.
[22] F.J. Quites, H.O. Pastore, Hydrothermal synthesis of nanocrystalline VO_2 from poly(diallyldimethylammonium) chloride and V_2O_5, Materials Research Bulletin 45 (2010) 892–896.
[23] S.D. Zhang, Y.M. Li, C.Z. Wu, F. Zheng, Y. Xie, Novel flowerlike metastable vanadium dioxide (B) micronanostructures: facile

synthesis and application in aqueous lithium ion batteries, Journal of Physical Chemistry C 113 (2009) 15058–15067.
[24] J.J. Huang, X.F. Wang, J.F. Liu, X.M. Sun, L. Wang, X.M. He, Flexible free-standing VO_2(B) nanobelts films as additive-free cathode for lithium-ion batteries, International Journal of Electrochemical Science 6 (2011) 1709–1719.
[25] C.V. Subha Reddy, E.H. Walker Jr., S.A. Wicker Sr., Q.L. Williams, R.R. Kalluru, Synthesis of VO_2(B) nanorods for Li battery application, Current Applied Physics 9 (2009) 1195–1198.
[26] M. Umeda, K. Dokko, Y. Fujita, M. Mohamedi, I. Uchida, J.R. Selman, Electrochemical impedance study of Li-ion insertion into mesocarbon microbead single particle electrode, Part I. Graphitized carbon, Electrochimica Acta 47 (2001) 885–890.
[27] H.M. Liu, Y.G. Wang, K.X. Wang, E. Hosono, H.S. Zhou, Design and synthesis of a novel nanothorn VO_2(B) hollow microsphere and their application in lithium-ion batteries, Journal of Materials Chemistry 19 (2009) 2835–2840.
[28] W.U. Huynh, J.J. Dittmer, A.P. Alivisatos, Hybrid nanorod–polymer solar cells, Science 295 (2002) 2425–2427.
[29] W.T. Jiang, J. Ni, K. Yu, Z.Q. Zhu, Hydrothermal synthesis and electrochemical characterization of VO_2(B) with controlled crystal structures, Applied Surface Science 257 (2011) 3253–3258.